

First-Principles Simulation of Scanning Tunneling Microscopy Images of Individual Molecules in Alkanethiol Self-Assembled Monolayers on Au(111)

Bin Li, Changgan Zeng, Qunxiang Li, Bing Wang, Lanfeng Yuan, Haiqian Wang, Jinlong Yang,* J. G. Hou,* and Qingshi Zhu

Structure Research Laboratory and Open Laboratory of Bond Selective Chemistry,
University of Science and Technology of China, Hefei, Anhui 230026, People's Republic of China

Received: May 25, 2002; In Final Form: October 17, 2002

The density functional theory calculations with local density approximation have been performed to simulate scanning tunneling microscopy (STM) images of individual molecules in close-packed upright alkanethiol self-assembled monolayers (SAMs) on a Au(111) surface. The internal patterns in the simulated STM images are dependent on bias voltage and alkanethiol chain length and have characteristics of the topographic effect modulated by the electronic effect. The electronic structure of the adsorption system is analyzed for discussing the STM imaging mechanism of alkanethiol SAMs. Besides enhancing the intermixing between the alkyl part and the Au substrate states, the sulfur atom in alkanethiol obviously influences the pattern in the STM image by its chemisorption mode on the Au(111) surface. Simulated images qualitatively reproduce STM experimental results.

I. Introduction

In recent years, self-assembled monolayers (SAMs) formed when organic molecules chemisorbed on substrates have been extensively studied¹ because of their potential applications as wetting controller,² biological sensors,³ membranes,⁴ nonlinear optical materials,⁵ molecular electronic devices,⁶ and so on. A typical example of the SAMs is alkanethiol chemisorbed on a Au(111) surface.^{7–10} A mass of experiments based on various diffraction, spectroscopy, and microscopy techniques has been used to characterize the molecule-scale structure of alkanethiol SAMs on Au(111).^{7,10} Also, some theoretical studies, such as the molecular dynamic (MD) simulation^{11–16} and the ground-state calculations,^{17–25} were carried out to simulate the interactions among components of alkanethiol SAMs system and reproduce the actual structure of alkanethiol SAMs. Although the basic structure of alkanethiol SAMs on Au(111) has been ascertained with quantitative precision,^{8,10} until now there still exist lots of controversies about the headgroup bonding structure, the packing configuration, and so on. STM has succeeded in studying the locally spatial and electronic structure of the conducting material surface, even with single-orbital resolution²⁶ and has always been expected to exert its high spatial resolution ability to explore the molecule-scale structure of SAMs, especially alkanethiol SAMs on Au(111). But STM studies for alkanethiol SAMs on Au(111) were not very satisfying,^{27–40} and there still exists much illegibility and divarication about the representations of various intramolecular patterns obtained in STM experiments. For example, some researchers persisted in the conventional viewpoint that only electrons directly tunneling through Au-bound sulfur contribute to tunneling current in STM imaging for alkanethiol SAMs,^{27,32,37,40} but some researchers argued that STM can detect the alkyl part of alkanethiol molecules though apparently no state belonging to the alkyl part is available for electron tunneling.^{28,39}

In fact, the illegibility and divarication occurring in STM studies for alkanethiol SAMs is because we have not explicitly understood the STM imaging mechanism itself and the nature of molecules–substrate interaction, even though alkanethiol SAMs are almost the simplest self-assembly system. For example: What information does the patterns in STM image of alkanethiol SAMs reflect? How does electron tunnel through the insulating alkyl chain? How does the adsorption mode of molecule influence the tunneling process and STM image? And what role does the sulfur exert in STM experiments for alkanethiol SAMs? These interesting questions still need more theoretical work although some related studies had already been done.^{41–44} Settling these questions also helps to comprehend properties of electron tunneling through organic molecules adsorbed on surfaces,^{45,46} even other complex molecule systems, and to evaluate the effect of interactions between molecule and substrate on them.

Recently we have observed high-resolution STM images of decanethiol and heptanethiol close-packed upright SAMs on a Au(111) surface and related the patterns with different spatial configurations of the topmost parts of alkanethiol molecules by combining STM experimental results and the density functional theory (DFT) calculations with the local density approximation (LDA).⁴⁷ It indicates that the LDA theoretical calculation is fit for recognizing patterns in STM images of alkanethiol SAMs. In this paper, we extend our work by further simulating STM images of individual molecules in alkanethiol SAMs on Au(111) surface with various possible structural parameters and configurations. The electronic structure of the alkanethiol molecules adsorption system is calculated and analyzed, and the STM imaging mechanism of three-dimensional (3-D) insulated organic molecules chemisorbed on a metal substrate is also discussed considering alkanethiol SAMs as a typical example. The systemically simulated results not only give out the chain length dependence and bias voltage dependence of the patterns in STM images of individual molecules in alkanethiol SAMs but also show that the sulfur adsorption mode

* Corresponding authors. E-mail: J.Y., jlyang@ustc.edu.cn; J.G.H., jghou@ustc.edu.cn.

on Au(111) is important to the voltage-dependent patterns in STM images for alkanethiol SAMs besides helping to produce appreciable tunneling current.

II. Computational Method and Structural Model

In general, the observed internal pattern of STM image for the sample is not directly related to the internal atomic configuration but to the electronic structure of sample surface.⁴⁸ We adopted Tersoff and Hamann's formula⁴⁹ and its extension to simulate STM images. In this method, the tunneling current in the STM can be expressed as

$$I(V) \propto \int_{E_F}^{E_F + eV} \rho(\vec{r}, E) dE \quad (1)$$

$$\rho(\vec{r}, E) = \sum_i |\psi_i(\vec{r})|^2 \delta(E - E_i) \quad (2)$$

where $\rho(\vec{r}, E)$, $\psi_i(\vec{r})$, and E_F are the local density of states (LDOS) of the sample, the sample wave function with energy E_i , and the Fermi energy, respectively. Equations 1 and 2 assume a constant density of states of the tip, which allows us to obtain STM images from only the LDOS of the sample surface. This assumption is tenable when the separation between the tip and sample is big enough, which accords with the situation in high tunneling-junction impedance STM experiments for alkanethiol SAMs. It is known that the LDOS near the E_F makes a dominant contribution to STM images. Hence we can obtain the LDOS by adding up the square of eigenvectors within the energy range from E_F to $E_F + eV_S$ (V_S is bias voltage of the sample relative to STM tip in experiment) with the same weight. By this method, we have already succeeded in simulating the STM image of individual C_{60} on a Si(111)-(7×7) surface that are consistent with experimental results.⁴⁸

It is well-known that, when the coverage reaches saturation, the alkanethiol monolayer is commensurate with the underlying Au lattice and is a $\sqrt{3} \times \sqrt{3}R30^\circ$ hexagonal overlayer or $c(4 \times 2)$ superlattice of the hexagonal lattice.^{8,10,28–30,50–53} The interaction between alkanethiol molecules is predominantly van der Waals, which should not markedly influence the charge distribution around alkanethiol molecules, so it is appropriate to consider only an individual alkanethiol in our model for the theoretically simulating STM image. The orientational configurations of alkanethiol molecules in SAMs are determined by the sulfur–Au substrate interaction and long-range van der Waals force between the hydrocarbon chains. There are six parameters determining geometry configuration of the alkanethiol molecule adsorbed on the Au(111) surface (the definitions of some important orientational structural parameters are shown in Figure 1):

1. The adsorption site of the sulfur atom on Au(111) surface: The conventional viewpoint was that sulfur atoms of alkanethiol molecules stand on the hollow site of the Au(111) surface with an S–S spacing of 4.99 Å.^{17,21,50–52,54–56} Recently some theoretical studies brought debates about this viewpoint^{21–25} and proved that the bridge site adsorption configuration of sulfur is the most stable.^{22–25} But the latest HREELS experiment showed that multiple adsorption sites of sulfur may exist in actual alkanethiol SAMs.⁵⁷ In this paper we start with the classical hcp site (one of hollow sites) adsorption model and consider fcc site (another hollow site) and bridge site adsorption cases later.

2. The chain length of the alkanethiol molecule (or the number (n) of carbon atoms): Up to now, the alkanethiol SAMs, which can present clear patterns in STM experiments, have carbon

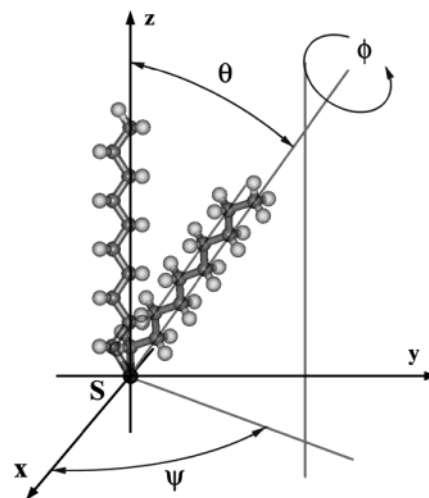


Figure 1. Schematic of angular degrees of freedom of alkanethiol (bound to substrate via sulfur group) in SAMs on Au(111). The x – y plane is parallel to the Au(111) surface, and the x axis is usually defined as the next-nearest neighbor molecule direction. Angle θ refers to the tilt of the molecular axis with respect to the substrate surface normal. Angle ψ defines the tilt direction; i.e., it is derived from projection of the molecule in the substrate plane. The twist angle ϕ describes rotation about the axis of the molecule.

number n from 4 to 18.^{27–40} In fact, the tunneling current values through (standing-up) hydrocarbon chains are appreciable only for n -alkanethiol SAMs with $n \leq 18$.^{27,44} So in this paper we only simulate STM images of alkanethiol SAMs with $4 \leq n \leq 18$.

3. The tilt angle θ of alkanethiol molecule: Almost all experimental and theoretical results about alkanethiol SAMs on Au(111) agreed that the tilt angle θ of carbon chain is $\sim 30^\circ$.^{8,10}

4. The tilt direction of the alkanethiol molecule: Diffraction experiments indicated that the tilt direction exhibits a trend of shifting away from the next-nearest neighbor (NNN) direction toward the nearest neighbor (NN) direction with chain lengths shortened.⁵⁸ In fact, our simulation results will show that the tilt direction of the alkanethiol molecule does not influence the pattern of simulated STM images of the alkanethiol molecule adsorbed on Au(111).

5. The twist angle ϕ of the hydrocarbon chains of the alkanethiol molecule about their molecular axes: An early IR experimental result showed that the ϕ value is about 55° .⁵¹ MD simulation results agreed that ϕ is about ± 35 – 55° or ± 125 – 145° for the alkanethiol molecule in the $c(4 \times 2)$ superlattice of SAMs.^{12,16} In the following calculations, we set ϕ to $\pm 45^\circ$ and $\pm 135^\circ$, and the influence of derivation from these average values of ϕ will be evaluated.

6. The existence of gauche defect or not: If there exist the gauche defects for alkanethiol molecules, the distributing status of the gauche defects in SAMs will be very complicated,^{14,59–61} which will make quantitative calculation more difficult. So in this paper, the alkanethiol molecule is only considered as a classical all-trans zigzag chain. Accordingly, the sulfur-dimer structure model induced by the annealing process⁶² is not considered because it demands the gauche defects.

So we first consider a model composed of a single n -alkanethiol molecule with an all-trans chain adsorbed on the hcp site of the Au(111) surface: $n = 7$; $\theta = 30^\circ$; tilt direction is NNN direction; $\phi = \pm 45^\circ$ and $\pm 135^\circ$. Subsequently, we will change the values of some parameters and evaluate the possible effect of their variation on the simulated STM images of alkanethiol SAMs on the Au(111) surface.

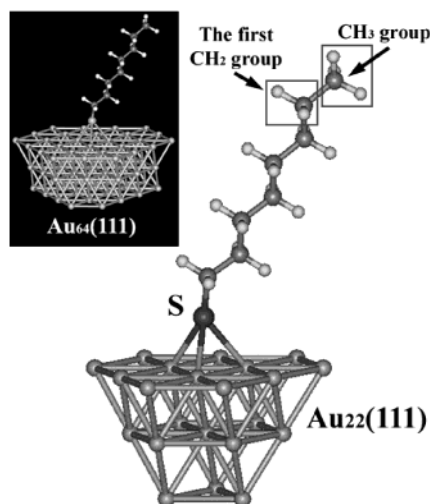


Figure 2. Cluster model of the alkanethiol molecule adsorbed on the hcp site of the Au(111) surface for simulating STM images, in which the Au surface is mimicked by 22 Au atoms. (Inset: cluster model in which Au surface is mimicked by 64 Au atom.)

For the substrate structure, we adopt a 22-atom Au cluster to mimic the Au(111) surface, which is arranged to three layers with closest-packed array (Figure 2). To verify the validity of this cluster model, we also perform STM image simulation with a cluster including 64 Au atoms (insert in Figure 2), and the results are qualitatively unchanged relative to those by the cluster model only including 22 Au atoms.

Our calculations for the electronic structures are performed using the DFT⁶³ as implemented in the DMol package.⁶⁴ At the LDA level, we choose the Vosko–Wilk–Nusair (VWN) local correlation functional⁶⁵ using parametrizations of Ceperley and Alder’s electron gas Monte Carlo data.⁶⁶ The double numerical DFT atomic orbitals augmented by polarization functions are used as the variational basis set for the valence electrons, whereas the core electrons are treated as frozen cores to save the computation effort without significantly sacrificing the accuracy. The electronic structure is obtained by solving the Kohn–Sham equations self-consistently in the spin-polarized

scheme. The self-consistent field procedure is carried out with a convergence criterion of 10^{-5} au on the energy and electron density. We optimized only the heights of the alkanethiol molecules above the Au(111) surface. For a 7-alkanethiol molecule adsorbed on the hcp site of the Au(111) surface, we obtained the optimized distance of sulfur atom from Au surface 2.05 Å, which is between Sellers et al.’s (1.91 Å),¹⁷ Yourdshahyan et al.’s (1.831 Å),²¹ and Beardmore et al.’s result (2.34 Å),¹⁸ and very close to Akinaga et al.’s calculation value (2.09 Å).²² The LDOS distribution on the plane with a height about 3.5 Å above the topmost methyl group of the alkanethiol was calculated for simulating the STM tunneling current image with constant height mode.

III. Simulation Results

A. 7-Alkanethiol Adsorbed at the hcp Site of Au(111).

Figure 3 shows simulated STM images of a single 7-alkanethiol molecule in SAMs under three bias voltage conditions ($V_s = -1.0, +1.0$, and $+2.0$ V), and with four orientational configurations ($\phi = \pm 45^\circ$ and $\pm 135^\circ$), respectively. These three bias voltage values cover the typical variation range of the bias voltage used in STM experiments and, more importantly, represent the main variation trend of the patterns in our simulated STM images (the STM images with $V_s = -2.0$ and 0 V are very similar to those with $V_s = -1.0$ and $+1$ V, respectively, so they are not shown). The patterns of all simulated STM images are round spot, elliptical spot, or dimer consisting of two spots, as observed in usual STM experiments.^{27–40} The projections of all these patterns on the alkanethiol adsorption system are situated on the terminal parts of hydrocarbon chain of alkanethiol molecule (Figure 4). This is opposite to the conventional argument that the patterns in STM images of alkanethiol SAMs on Au(111) are the reflection of Au-bound sulfur atoms.^{27,32,37,40} To display our conclusion more distinctly, we calculated and compared two line profiles of the LDOS versus distance from Au(111) surface with V_s equal to 1.0 V, and these two lines are vertically through the center of the terminal methyl (CH_3) group and sulfur atom, respectively (Figure 5). From it we can see that under the usual STM work mode (tip does not penetrate into the alkanethiol monolayer),

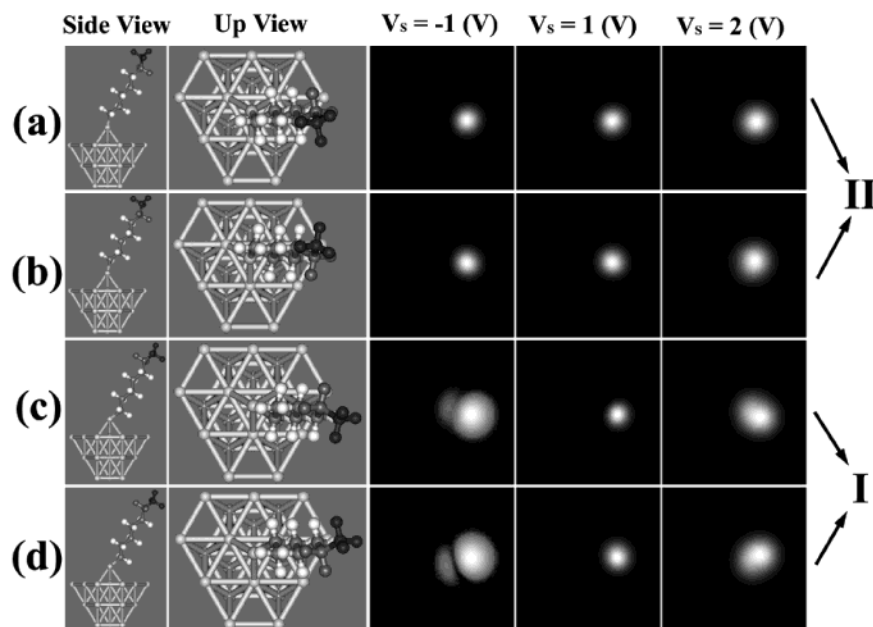


Figure 3. Two views and simulated STM images with $V_s = -1.0, +1.0, +2.0$ (V) for four orientations of individual molecules in 7-alkanethiol SAMs on Au(111). The twist angle ϕ of the hydrocarbon chain: (a) $+45^\circ$, (b) -45° , (c) $+135^\circ$, (d) -135° .

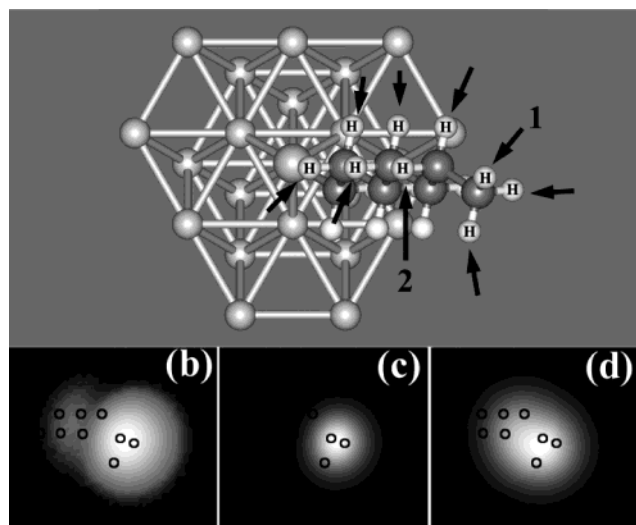


Figure 4. Contrast between the structural model (a) and simulated STM images (b–d) of 7-alkanethiol on Au(111), with the twist angle $\phi = 135^\circ$; (b) simulated STM images with $V_s = -1.0$ (V); (c) simulated STM images with $V_s = 1.0$ (V); (d) simulated STM images with $V_s = 2.0$ (V).

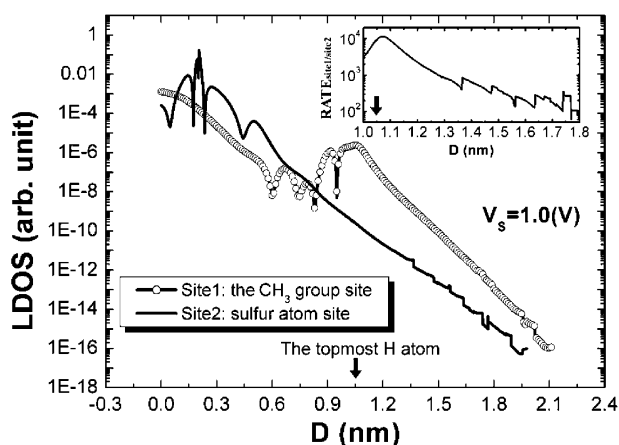


Figure 5. Vertical line profile of calculated LDOS versus distance from the Au(111) surface ($V_s = 1.0$ (V)). Two curves represent LDOS on two vertical lines through the terminal CH_3 group and sulfur atom, respectively. Arrow indicates the height of the topmost H atom from Au surface. (Inset: the rate between LDOS values of two line profiles versus distance.)

the LDOS detected by the tip upon the terminal CH_3 group are thicker than that upon the sulfur atom (also see inset in Figure 5), which results in the bright spot in the STM image appearing at the position upon the terminal part of hydrocarbon chain according to Tersoff–Hamann theory.⁴⁹

Another remarkable phenomenon is the bias voltage dependence of the pattern in the STM image. For the orientational configurations with $\phi = \pm 45^\circ$, the patterns are always one bright round spot and are not bias voltage dependent. But the patterns for the orientational configurations with $\phi = \pm 135^\circ$ are dependent on the bias voltage: when V_s is from -2.5 to -0.5 V (-1.0 V as representation), the patterns are a dimer consisting of two bright spots; when V_s is changed from -0.5 to $+1.5$ V ($+1.0$ V as representation), the patterns are one bright round spot; when V_s is increased to about $+1.5$ – 2.5 V ($+2.0$ V as representation), the patterns turn to bright elliptical spot. In Figure 6a, three line profiles for the cross-sections marked by the lines in Figure 6b quantitatively show the difference between the patterns of STM images under $V_s = -1.0$, $+1.0$, and $+2.0$ V for the orientation configurations with $\phi = 135^\circ$. The peak

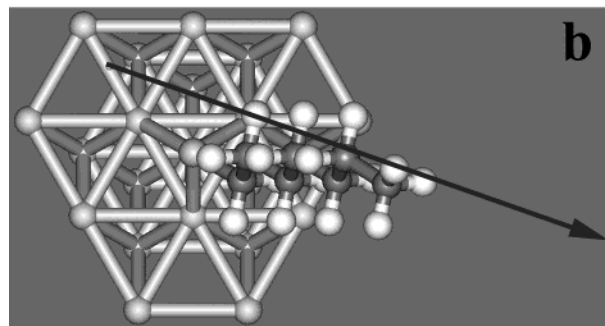
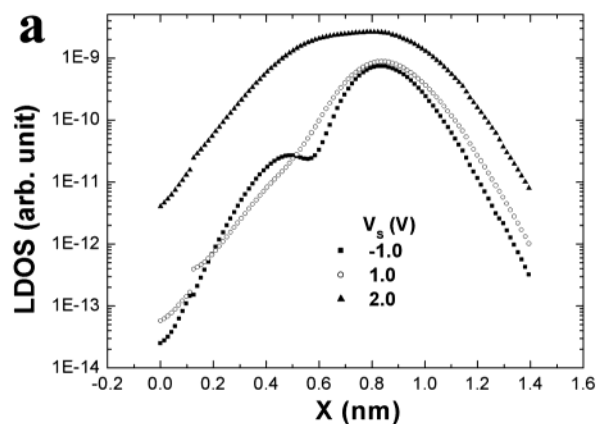


Figure 6. (a) Line profile for the cross-section of the bright spots dimer marked by a directional line in (b). (b) Top view of the structural model of 7-alkanethiol on Au(111) with $\phi = 135^\circ$.

of line profile curve under $V_s = 2.0$ V is flatter than that under other two bias voltages and extends to one side. It is found that the projection of the bright round spot on the alkanethiol adsorption system under low positive bias voltage is situated on the terminal CH_3 group, the projection of the extension part of pattern in STM image under 2.0 V bias voltage is mainly situated on the first methylene (CH_2) group next to the terminal CH_3 group, and the projection of the second bright spot appearing under -1.0 bias voltage is situated on the superposition part of the first, third, and even fifth CH_2 groups (Figure 4).

B. Alkanethiol Adsorbed at the hcp Site of Au(111) with Different Chain Lengths. Also, we have simulated STM images of an 8-alkanethiol molecule in SAMs. Figure 7 shows simulated STM images of a single 8-alkanethiol molecule in SAMs under three bias voltage conditions for four orientational configurations corresponding to $\phi = \pm 45^\circ$ and $\pm 135^\circ$, respectively. Being different from the case for 7-alkanethiol, the voltage dependence of the STM image does not appear for the orientational configurations with $\phi = \pm 135^\circ$ but exists for those with $\phi = \pm 45^\circ$: the patterns are one bright round spot when V_s is from -2.5 to $+1.7$ V (no dimer pattern appears), and when V_s is increased to about 1.7 – 2.5 V, the patterns turn to bright elliptical spot.

We further simulated STM images of the n -alkanethiol molecule in SAMs, with n from 4 to 18, and still concentrated on the bias voltage dependence of the pattern in the STM image. Similarly, we found that the bias voltage dependence only appears in the simulated STM images for the following orientational configurations: the configurations with $\phi = \pm 135^\circ$ when the carbon atom number n is odd, and the configurations with $\phi = \pm 45^\circ$ when n is even. We denoted the above orientational configurations as configurations I, and the following orientational configurations were denoted as configurations II: the configurations with $\phi = \pm 45^\circ$ when the carbon atom

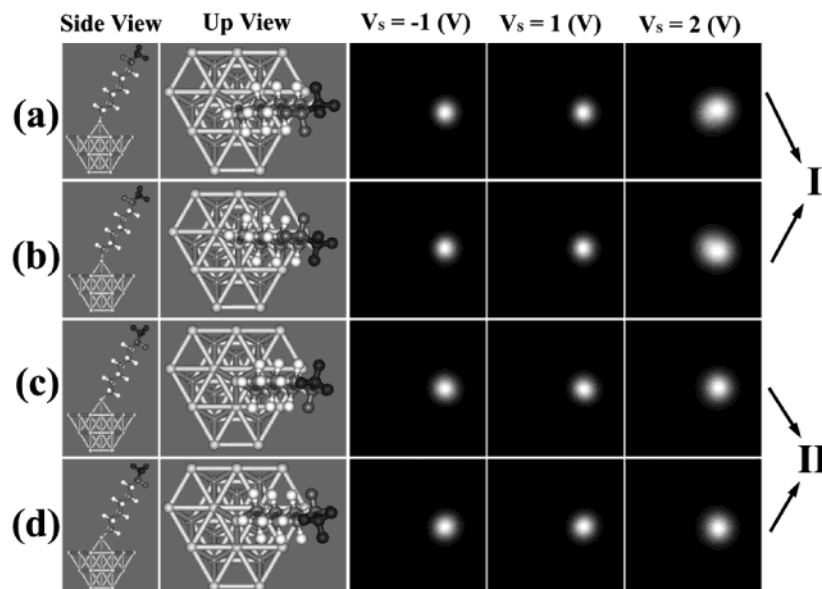


Figure 7. Two views and simulated STM images with $V_s = -1.0, +1.0, +2.0\text{ (V)}$ for four orientations of individual molecules in 8-alkanethiol SAMs on Au(111). The twist angle ϕ of the hydrocarbon chain: (a) $+45^\circ$, (b) -45° , (c) $+135^\circ$, (d) -135° .

number n is odd, and the configurations with $\phi = \pm 135^\circ$ when n is even. In the simulated STM images for configurations II, the patterns are always one bright round spot and are not voltage-dependent. So we only considered configurations I in the following. Furthermore, because the voltage dependences of patterns in STM images are the same for the orientational configurations with $\phi = +45^\circ$ and -45° (or $+135^\circ$ and -135°), we only consider the orientational configurations with ϕ equal to 45° or 135° . All simulated STM images for configurations I are shown in Figures 8–10, and we can find the following characteristics:

1. When the carbon atom number n is between 6 and 11, the voltage dependence of the pattern in the STM image presents itself as the odd–even effect (Figure 8): for even-carbon-atom-number alkanethiol ($n = 6, 8, 10$), when V_s is from -2.5 V to $+1.7\text{ V}$, the patterns are one bright round spot, and when V_s is increased to about $1.7\text{--}2.5\text{ V}$, the patterns are one bright elliptical spot; for odd-carbon-atom-number alkanethiol ($n = 7, 9, 11$), when V_s is from -2.5 to -0.5 V , the patterns are one dimer consisting of two bright spots (in the $n = 11$ case, the second bright spot is so dominant that the pattern looks like an elliptical spot), when the bias voltage is changed to from -0.5 to $+1.5\text{ V}$, the patterns turn to one bright round spot, and when V_s is increased to about $1.5\text{--}2.5\text{ V}$, the patterns turn to one bright elliptical spot. The projections of all of one bright round spot patterns on the alkanethiol adsorption system are situated on the terminal CH_3 group, and the projections of all of the second bright spots or the extensions of the first bright spot are situated on the first CH_2 group or the superposition part of the first, third, and even fifth CH_2 groups. Namely, when V_s is from -0.5 to $+2.5\text{ V}$, the voltage dependences of patterns in the STM images are similar for the alkanethiol adsorption system with odd and even carbon atom numbers, showing that the information of the terminal CH_3 group and the first CH_2 group can be simultaneously detected at $V_s > 1.7\text{ V}$, but when V_s is negative, the information of the CH_2 groups can be detected only in the alkanethiol adsorption system with odd carbon atom numbers. This special odd–even effect needs theoretical interpretation.

2. When we further increased n to 12 and more, the difference between the patterns in simulated STM images under various bias voltage conditions for various orientational configurations

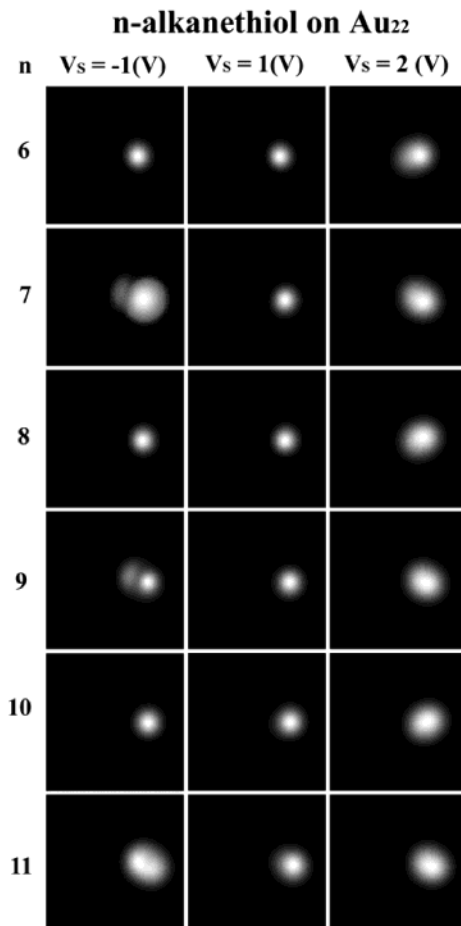


Figure 8. Simulated STM images with $V_s = -1.0, +1.0, +2.0\text{ (V)}$ for individual molecules in n -alkanethiol SAMs on Au(111), with $6 \leq n \leq 11$. The twist angle ϕ is 45° for even n , and 135° for odd n .

gradually becomes inconspicuous and even disappears (Figure 9): all patterns in STM images are similar and only one round bright spot can be resolved. Actually, this trend can also be found in the case with $n = 11$. This implies that the STM experiment is difficult to distinguish between different orientational configurations of long-chain alkanethiol molecules in SAMs.

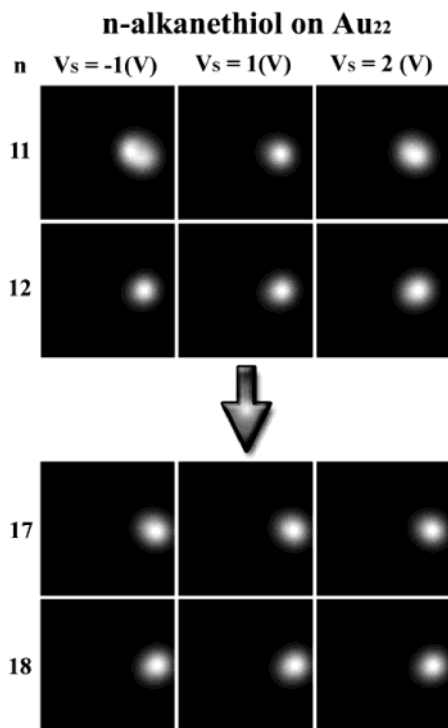


Figure 9. Simulated STM images with $V_s = -1.0, +1.0, +2.0$ (V) for individual molecules in *n*-alkanethiol SAMs on Au(111), with $n = 11, 12, 17, 18$. The twist angle ϕ is 45° for even n , and 135° for odd n .

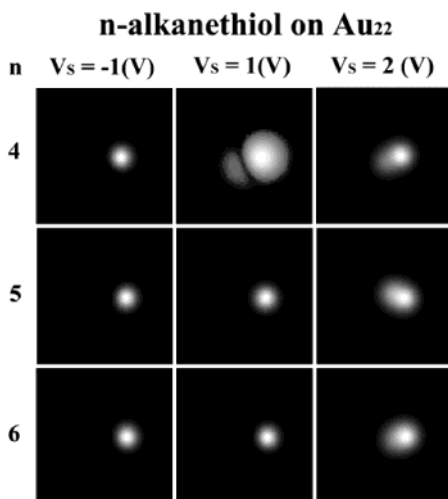


Figure 10. Simulated STM images with $V_s = -1.0, +1.0, +2.0$ (V) for individual molecules in *n*-alkanethiol SAMs on Au(111), with $4 \leq n \leq 6$. The twist angle ϕ is 45° for even n , and 135° for odd n .

3. Similarly, the odd-even effect disappears when the number n of carbon atoms is decreased to 5 and 4 (Figure 10). We can find that in the STM image for the 5-alkanethiol adsorption system the pattern is a bright round spot when V_s is -1.0 V, and in the STM image for 4-alkanethiol adsorption system the pattern is a dimer when V_s is 1.0 V. These patterns are all different from those in *n*-alkanethiol adsorption with $6 \leq n \leq 11$. In addition, we originally expected that the Au-bound sulfur atom can be seen in the simulated STM image for the shorter chain length *n*-alkanethiol adsorption system, but the simulated results showed that the LDOS value upon the sulfur site is still very small with respect to that upon the terminal CH_3 group site, even in the case with $n = 4$.

C. Effects of Other Parameters. As mentioned above, there are lots of uncertainties and alternatives for quantitative values

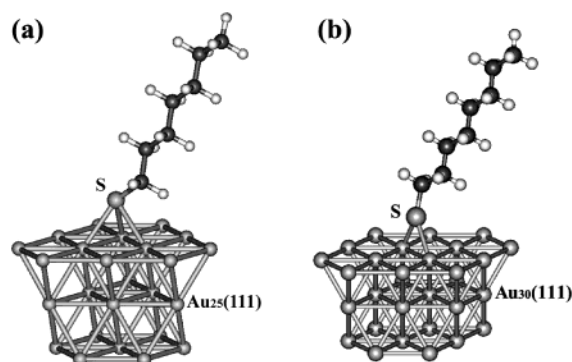


Figure 11. Cluster model of alkanethiol molecule adsorbed on (a) fcc and (b) bridge sites of the Au(111) surface for simulating STM images, in which the Au surface is mimicked by 25 and 30 Au atoms, respectively.

of structural parameters of alkanethiol molecules adsorbed on Au(111). In the following, the effects of several structure parameters of the *n*-alkanethiol molecule adsorption system on the pattern in the simulated STM image will be evaluated:

1. Adsorption Site of *n*-Alkanethiol Molecule. Although not correctly describing long range interaction, some groups recently performed DFT calculations of CH_3S molecules adsorbed on the Au(111) surface and showed that the fcc or bridge sites adsorption are possibly more stable than hcp site adsorption of the alkanethiol molecule.^{21–25} We changed the adsorption site of the sulfur atom of the alkanethiol molecule in the above adsorption configurations to the fcc site, and a cluster consisting of 25 Au atoms was adopted to mimic Au(111) surface in this case (Figure 11a). The simulated results show the voltage dependence of the pattern in the STM image still appears only for configurations I. In configurations I, for even-carbon-atom-number alkanethiols, the patterns are one bright round spot when V_s is from -2.5 to $+1.7$ V and are one bright elliptical spot when V_s is from 1.7 to 2.5 V; for odd-carbon-atom-number alkanethiols, the patterns are one dimer consisting of two bright spots when V_s is from -2.5 to -0.5 V, are one bright round spot when V_s is from -0.5 to $+0.7$ V, are one dimer when V_s is from 0.7 to 1.5 V, and are one bright elliptical spot when V_s is from 1.5 to 2.5 V. As typical examples, the simulated STM images for configurations I with $n = 8$ and 9 are shown in Figure 12a. We can find that there is no distinct difference between the patterns in STM images of two kinds of configurations with different sulfur adsorption sites for even-carbon-atom-number alkanethiols, and the differences between the patterns appear when the carbon atom number of the alkanethiol is odd (such as $n = 9$ in Figure 12a), especially that the pattern is a dimer when V_s is from 0.7 to 1.5 V with fcc adsorption site, whereas it is one round spot with hcp adsorption site.

To study the case for bridge site adsorption, we choose a cluster consisting of 30 Au atoms to mimic the Au(111) surface (Figure 11b), and the simulated results also show only configurations I have the voltage dependence of the pattern in the STM image. For even-carbon-atom-number alkanethiols, the patterns are one bright round spot when V_s is from -2.5 to $+1.1$ V and are one bright elliptical spot when V_s is from 1.1 to 2.5 V; for odd-carbon-atom-number alkanethiols, the patterns are one dimer consisting of two bright spots when V_s is from -2.5 to -1.0 V, are one bright round spot when V_s is from -1.0 to $+1.1$ V, and are one bright elliptical spot when V_s is from 1.1 to 2.5 V. In Figure 12b, the simulated STM images for configurations I with $n = 8$ and 9 are shown as typical examples. It can be found that the bias voltage dependence of the STM image is different from that for the hcp site adsorption

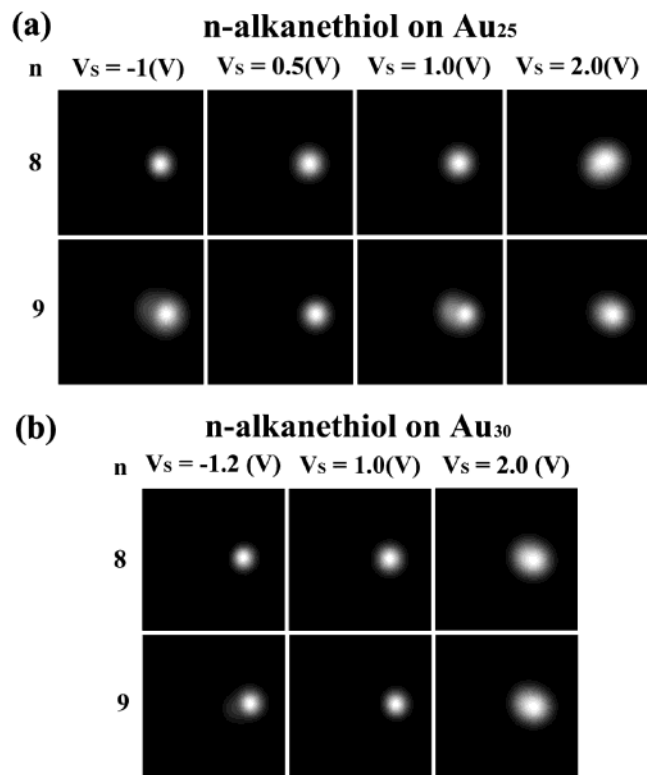


Figure 12. (a) Simulated STM images with $V_s = -1.0, +0.5, +1.0, +2.0$ (V) for individual molecules in n -alkanethiol SAMs on the fcc site of Au(111), with $n = 8, 9$. The twist angle ϕ is 45° for even n , and 135° for odd n . (b) Simulated STM images with $V_s = -1.2, +1.0, +2.0$ (V) for individual molecules in n -alkanethiol SAMs on the bridge site of Au(111), with $n = 8, 9$. The twist angle ϕ is -45° for even n , and -135° for odd n .

case with two points: one is that the bias-voltage thresholds where the patterns of simulated STM images vary are different from those for the hcp site adsorption case; another is that the smaller spot is difficult to be resolved in the STM image for odd-carbon-atom-number alkanethiol SAMs when V_s is from -2.5 to -1.0 V.

2. Tilt Direction of the Alkanethiol Molecule. We choose the 9-alkanethiol adsorption system with $\phi = 135^\circ$ as an example to study the dependence of STM images on the tilt direction of the alkanethiol molecule. Owing to C_{3v} symmetry at the hollow site of the Au(111) surface, we set the tilt direction of the alkanethiol molecule from one NNN direction to its next equivalent NNN direction with a 10° interval, i.e., totally 12 orientational configurations. From the simulated STM images (not being shown), we can find that the pattern in the STM image remains invariable except for rotating around the sulfur atom site. Other n -alkanethiol adsorption systems with different n and ϕ values also give the same result.

3. Twist Angle of the Hydrocarbon Chains about Their Molecular Axes. As already mentioned, the twist angle of the hydrocarbon about their molecular axes ranges from $\pm 35^\circ$ to 55° and from $\pm 125^\circ$ to 145° , according to MD simulation results. To evaluate the influence of the twist angle deviating from the average value ($\pm 45^\circ$ and $\pm 135^\circ$) on the pattern in the STM image, the hcp site adsorption system of 7-alkanethiol on the Au₂₂(111) cluster with the twist angle equal to $\pm 35^\circ, \pm 40^\circ, \pm 45^\circ, \pm 50^\circ, \pm 55^\circ$ and $\pm 125^\circ, \pm 130^\circ, \pm 135^\circ, \pm 140^\circ, \pm 145^\circ$, i.e., a total of 20 orientational configurations, were adopted to calculate. Simulated results showed that in the range of the average twist angle with $\pm 10^\circ$, the pattern in the STM image (not being shown) does not vary markedly.

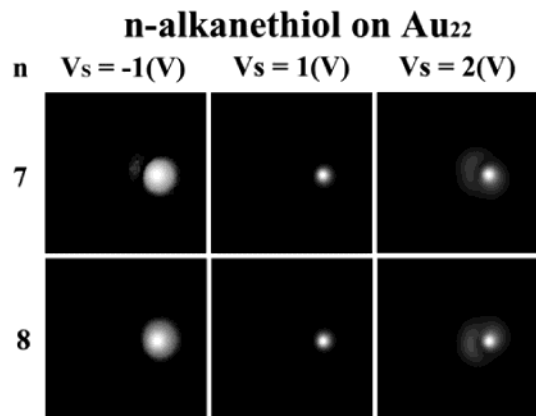


Figure 13. Simulated STM images with $V_s = -1.0, +1.0, +2.0$ (V) for individual molecules in n -alkanethiol SAMs on Au(111), with $n = 7, 8$. The twist angle ϕ is 45° for even n , and 135° for odd n . The tip-alkanethiol SAMs separation is taken as 1.5 \AA .

Furthermore, the separation distance between the STM tip and alkanethiol SAMs possibly affects the pattern in the STM image. The commonly accepted separation distance between the tip and sample is $3\text{--}5 \text{ \AA}$,⁶⁷ but some studies argued that a smaller separation distance is necessary to produce enough tunneling current through alkanethiol SAMs.⁴⁶ So we changed the height of the plane on which the LDOS distribution was calculated for simulating the STM image from about 3.5 \AA to 1.5 \AA above the topmost CH₃ group of the alkanethiol, and the simulated STM images for 7- and 8-alkanethiol with configurations I are shown in Figure 13. The basic properties of the patterns in images are similar to those with the height of the plane equal to 3.5 \AA , except the patterns under $V_s = 2.0$ V, which is a dimer, different from an elliptical spot in cases with the height of plane equal to 3.5 \AA . Moreover, the projections of these patterns on the alkanethiol adsorption system still are situated on the terminal CH₃ group and the first CH₂ group next to it. It is noticeable that the ratio of the LDOS value upon the first CH₂ group with respect to that upon the CH₃ group decreases distinctly. In Figure 14, two groups of the normalized line profiles of the LDOS for the cross-sections marked by the lines in Figure 6b show this trend for the patterns of STM images of the 7-alkanethiol adsorption system under $V_s = -1.0$ and $+2.0$ V with the orientation configurations with $\phi = 135^\circ$. This should behave itself in STM experiments as follows: the information of the first and other CH₂ groups is difficult to detect when the STM tip approaches alkanethiol SAMs.

IV. Analysis and Discussion

A. Electronic States Analysis of the Adsorption System.

To study the tunneling mechanism for alkanethiol SAMs in STM experiments and other related questions, it is necessary to analyze the electronic structure of the whole adsorption system. The alkanethiol molecule undergoes the breakdown of the sulfur-hydrogen bond before it is adsorbed on the Au(111) surface,⁹ so we considered the following four systems: 7-alkane molecule (CH₃-(CH₂)₅-CH₃, denoted as system A), 7-alkanethiol molecule (HS-(CH₂)₆-CH₃, denoted as system B), 7-alkanethiol molecule with a hydrogen atom being desorbed from the sulfur atom (S-(CH₂)₆-CH₃, denoted as system C), and 7-alkanethiol (S-(CH₂)₆-CH₃) adsorbed on the Au(111) surface (denoted as system D). Parts a-d of Figure 15 are the calculated total density of states (TDOS) and the partial density of states (PDOS) plot for sulfur atom and the terminal CH₃ group in these four systems.

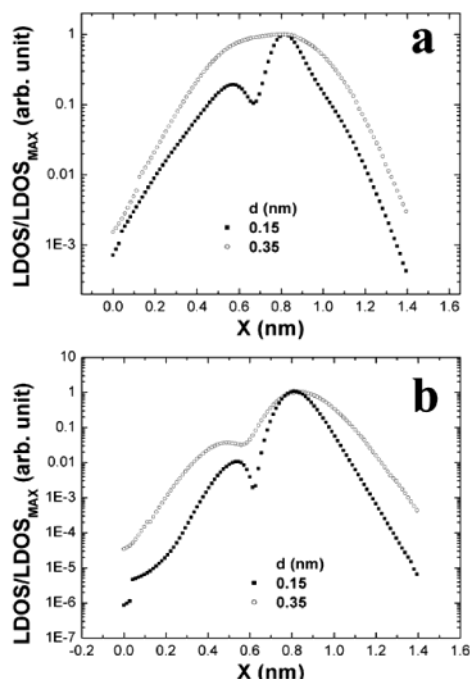


Figure 14. Two groups of the normalized line profiles of the LDOS for the cross-sections marked by the lines in Figure 6b showing the difference between the patterns in STM images of 7-alkanethiol adsorption system with the same $\phi = 135^\circ$ and different tip–alkanethiol SAMs separation d : (a) $V_s = 2.0$ V; (b) $V_s = -1.0$ V.

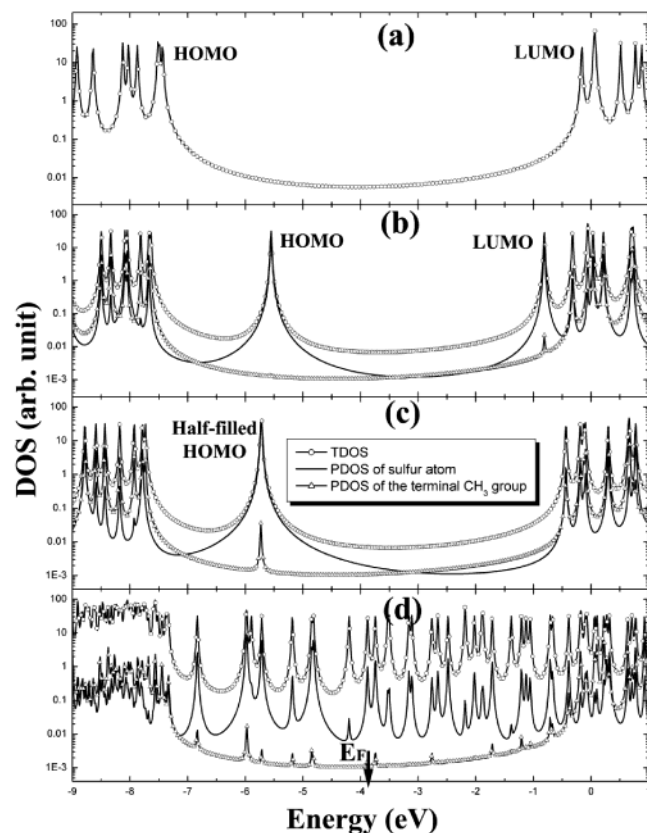


Figure 15. TDOS and PDOS plots for four systems, (a) 7-alkane ($\text{CH}_3-(\text{CH}_2)_5-\text{CH}_3$) molecule, (b) 7-alkanethiol ($\text{HS}-(\text{CH}_2)_6-\text{CH}_3$) molecule, (c) $\text{S}-(\text{CH}_2)_6-\text{CH}_3$, and (d) $\text{S}-(\text{CH}_2)_6-\text{CH}_3$, adsorbed on the Au(111) surface, respectively.

It is well-known that there is a big gap (of ~ 7.3 eV in our calculation) between the highest occupied molecular orbital (HOMO) and the lowest unoccupied molecular orbital (LUMO)

of the 7-alkane molecule. So the large HOMO–LUMO gap theoretically results in forbiddance of electrons tunneling with energy in the HOMO–LUMO gap of the alkane molecule and makes alkane molecules insulating (system A). The obtained tunneling current is not appreciable, and the electrons tunnel directly through molecule, not reflecting the molecular orbitals' information. So it is difficult to image alkane molecules in usual STM experimental conditions.

As for the 7-alkanethiol molecule, considered with the H– group replaced by an HS– group, a state with energy of -5.55 eV as the HOMO of the alkanethiol molecule emerges in the original HOMO–LUMO gap of the alkane molecule and is mainly dominated by the sulfur component. Due to the bonding interaction between sulfur and the hydrocarbon chain, the terminal CH_3 group also contributes to this new state. But there still are a HOMO–LUMO gap of ~ 4.7 eV, and the percentage of sulfur atomic orbitals in the HOMO and LUMO is more than that of the terminal CH_3 group orbitals (system B) by 4 orders of magnitude. So the emergence of this new state does not change the situation that the electrons with energy in the HOMO–LUMO gap of the alkane molecule are difficult to tunnel through the hydrocarbon chain and cannot reflect the information of molecular orbitals (MOs).

During the adsorption process of the alkanethiol molecule onto the Au(111) surface, the sulfur–hydrogen bond is broken, so the sulfur atom becomes an active group and is bonded to the Au(111) surface. Compared with the case in the 7-alkanethiol molecule (system B), the percentage of terminal CH_3 group orbitals in the half-filled HOMO and LUMO of the 7-alkanethiol molecule with a hydrogen atom desorbed (system C) increases obviously, despite that sulfur atomic orbitals still dominate in the half-filled HOMO.

When the 7-alkanethiol molecule ($\text{CH}_3(\text{CH}_2)_6\text{S}$) has been adsorbed on Au(111) (system D), there occur huge varieties in the DOS, especially, lots of new orbitals appear in the original HOMO–LUMO and (HOMO–1)–HOMO gaps of the 7-alkanethiol molecule (i.e., the original HOMO–LUMO gap of the 7-alkane molecule). Most of these orbitals are from plain Au bulk states (the DOS in Figure 15 are plotted in logarithmic coordinates, and in fact, Au states dominate in all these orbitals). But in some new orbitals, the percentages of sulfur and alkyl states are obviously more than those in other orbitals. Such orbitals result from the intermixing of MOs and substrate states induced by the strong interaction between the alkanethiol molecule and the Au substrate. In other words, the electronic coupling between the alkanethiol molecule and the Au surface increases the DOS in the gap by the opening the tunneling channels of MOs that are far from E_F . It is the superposition near E_F of all these channels that controls the tunneling characteristics of the whole system, although the transport phenomenon remains out of resonance.⁶⁸ Electrons transiting through these MOs reflect their information, which enables STM imaging for alkanethiol SAMs. Charge transfer from the Au to sulfur atom determined the main properties of interaction between the alkanethiol molecule and the Au(111) surface. Therefore, sulfur atomic orbitals still contribute to the frontier orbitals more than alkyl orbitals in the adsorption system (system D).

B. STM Imaging Mechanism for Alkanethiol SAMs. From the above electronic structure analysis, we can find that the percentage of sulfur atom orbitals in the frontier orbitals is more than that of carbon–hydrogen components by several orders of magnitude for all systems that we have analyzed in the above subsection. So it is natural to think that the tunneling current is

mainly through a Au-bound sulfur atom in STM experiments, which was first proposed by Widrig et al.²⁷ and had ever become popular argument.^{32,37,40} But the high tunneling resistance STM experiments performed by Delamarche et al.²⁸ and subsequent STM experiments^{29,33,39} suggested that the pattern in STM images of alkanethiol SAMs reflects the information of the terminal alkyl group. In our simulated STM images, the projections of all patterns are situated on the terminal parts of the alkyl chains in alkanethiol molecules, especially the terminal CH₃ group and the CH₂ group next to it. The position correspondence between the spots in patterns and groups in alkanethiol molecules suggests these patterns reflect the information of the terminal parts of alkyl chains. This appears to argue against Widrig et al.'s traditional standpoint.²⁷ Actually in our calculations, the LDOS distribution on the plane with a height about 3.5 Å above the topmost methyl group of alkanethiol was used, which makes our simulated STM images to be of the high tunneling resistance STM experimental condition. Delamarche et al.²⁸ emphasized that the profit of high tunneling resistance is to preclude STM tip penetration into the monolayer and allow the undisturbed observation of the $c(4\times 2)$ superlattice. So our calculations validated that in the high tunneling resistance STM experiments for alkanethiol SAMs, the information detected by the STM tip indeed reflected the terminal part of the hydrocarbon chain of the alkanethiol molecule.

To explain that the information about the terminal part of hydrocarbon chain is dominant in high tunneling resistance STM experiments and our simulated STM images although the Au-bound sulfur orbitals contribute to the frontier orbitals of the whole adsorption system more than the carbon–hydrogen components do (see Figure 15d), not only the electronic effect but also the topographic effect should be considered. Actually, for another kind of alkanethiol SAMs with $(m\times\sqrt{3})$ structure,^{10,31,69–71} the sulfur atom is brighter than the hydrocarbon chain in the STM image according to experimental^{31,69–71} and theoretically simulated results.⁷² In this case, the alkanethiol molecular backbone is laying down flat on metal surface, so the height of the sulfur atom is almost the same as that of carbon and hydrogen atoms, which results in the pattern of the STM image being primarily determined by the electronic effect. But for alkanethiol SAMs with close-packed hexagonal structure, the alkanethiol molecule is chemisorbed on the Au(111) surface with a $\sim 30^\circ$ tilt angle from the surface normal, so the terminal part of the hydrocarbon chain of the alkanethiol molecule is closer to the STM tip than the Au-bound sulfur atom with ~ 8 Å height difference. Commonly, the LDOS in the vacuum beyond the materials surface decays quickly with increasing distance from the surface. Therefore, though the percentage of Au-bound sulfur atomic orbitals in the frontier orbitals is more than that of the orbitals of the terminal alkyl part by 2 orders of magnitude, when the electronic effect and the topographic effect are combined for consideration, the dominance of Au-bound sulfur orbitals in DOS is reversed, and in the region probed by the STM tip the electronic wave function is localized near the terminal part of hydrocarbon chain, as our simulated images and plots for LDOS (Figure 5) show. A similar mechanism works for the case of inert gas atoms that also have a large HOMO–LUMO gap adsorbed on metal surface.⁷³

C. Bias Voltage-Dependent Patterns in STM Images. In our simulated results, the bias voltage dependence appears only in STM images for configurations I. From the structural schematics, we can find that the most distinct difference between configurations II and I is orientational structure for the topmost

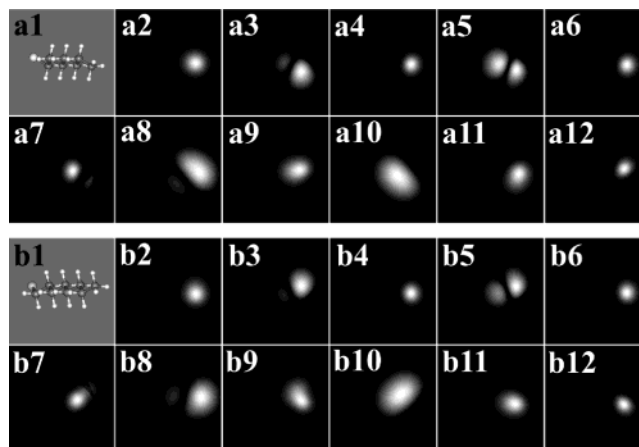


Figure 16. Calculated LDOS contours of MOs for 7- and 8-alkanethiol molecules with an H atom being desorbed (system C), of which the orientational configurations are kept the same as those in the adsorption system on Au(111) (system D) with $\phi = 135^\circ$ and 45° , respectively. (1) is top view of the structural model of alkanethiol molecules, and (2)–(12) correspond to HOMO(half-filled)-5 to LUMO+4 in turn.

groups of the hydrocarbon chain (Figures 3 and 7). So an obvious interpretation is the topographic effect: by reason of the zigzag structure of the alkanethiol molecule, the first CH₂ group is almost just below the terminal CH₃ group in configuration II, but in configuration I, the height of first CH₂ group is even closer to that of the terminal CH₃ group (Figures 3 and 7). So, for configurations II, the information of the first CH₂ group is cloaked by the terminal CH₃ group, so that cannot be found in STM images. Then the simulated STM images for configurations II are simple and have no bias voltage dependence. On the contrary, for configurations I, the information of the first CH₂ group is possible to detect by STM together with that of the terminal CH₃ group, as we have already showed.

Actually, the intermixing of the MOs of alkanethiol molecule with Au substrate states is also the origin of the bias voltage-dependent pattern in the simulated STM image for configurations I. In our simulation, the LDOS was obtained by adding the square of eigenvectors within the energy range determined according to the V_s value. So the voltage dependence of the pattern in the simulated STM image results from the energy-dependent spatial distribution of those new orbitals (system D) appearing in the original HOMO–LUMO and (HOMO–1)–HOMO gaps of 7-alkanethiol (system B). As mentioned above, some of these new orbitals result from the intermixing of the MOs and with Au substrate states with different mixing rates. Among these states, some appear near the original HOMO of alkanethiol, and their spatial distributions around the hydrocarbon chain are similar to the characteristic of the occupied orbitals of alkanethiol. And the spatial distributions of some new states close to the original LUMO of 7-alkanethiol are markedly influenced by the unoccupied orbitals of alkanethiol. As a visual illumination, Figure 16(a2–a12) shows calculated LDOS contours of MOs from HOMO(half-filled)-5 to LUMO+4 for the 7-alkanethiol molecule (CH₃(CH₂)₆S, system C), of which the orientational configuration is kept the same as those in the adsorption system on Au(111) (system D) with $\phi = 135^\circ$. And the contour planes are also the same as those in system D. By comparing the LDOS contours of these MOs with the simulated STM images in Figure 3, we can qualitatively understand the intermixing way into new states of alkanethiol MOs, i.e., how these MOs participate in the tunneling process out of resonance with different contributions. It is suggested that HOMO-2 and HOMO-4 predominantly contribute to the dimer pattern in the

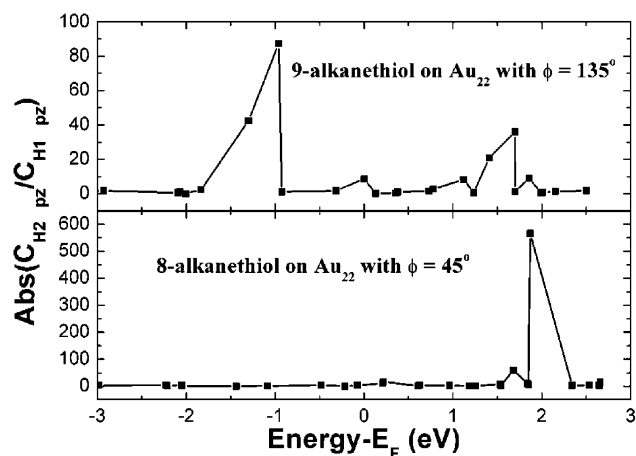


Figure 17. Absolute value of the ratio between the molecular orbital coefficients of the frontier orbitals on the hydrogen atom “2” p_z -like orbital and the hydrogen atom “1” p_z -like orbital, for two of configurations II (8-alkanethiol adsorbed on Au(111) with $\phi = 45^\circ$ and 9-alkanethiol adsorbed on Au(111) with $\phi = 135^\circ$).

simulated STM image for the 7-alkanethiol adsorption system under negative bias voltage, and the elliptical spot pattern under higher positive bias voltage may be related with the LUMO+2 and LUMO of alkanethiol (system C).

On the other hand, the bias voltage dependence of the spatial distributions of new orbitals can also be examined at the level of atomic orbitals. From Figure 4, we can find that hydrogen atom “1” (belonging to the terminal CH_3 group) and “2” (belonging to the first CH_2 group) are important for the formation of pattern in STM images, and they are closer to the STM tip than other atoms in groups. Figure 17 shows the absolute value of the ratio between our calculated molecular orbital coefficients of the frontier orbitals on the hydrogen atom “2” p_z -like orbital and the hydrogen atom “1” p_z -like orbital, for two types of configurations I (8-alkanethiol adsorbed on Au(111) with $\phi = 45^\circ$ and 9-alkanethiol adsorbed on Au(111) with $\phi = 135^\circ$). The variation trends of these two curves are consistent with those of patterns in STM images for two respective configurations: the orbitals for which the absolute values of the ratio are high appear in an energy region from which the information of the first CH_2 group begins to be detected in the STM image together with the terminal CH_3 group. Undoubtedly, the p_z -like orbital of the hydrogen atom is a dominating factor of the bias voltage dependence of the pattern in STM images.

D. Origin of the Odd–Even Effect of Patterns in STM Images. The difference between the bias voltage-dependent patterns (mainly under negative sample bias voltage) in the STM images for even-carbon-atom-number and odd-carbon-atom-number alkanethiol adsorption systems with configurations I when the carbon atom number is between 6 and 11, or the odd–even effect of the voltage-dependent pattern, is interesting, because their topmost groups structures are the same. It should result from the difference between electronic structures of two kinds of adsorption systems. In the above subsection, the molecular orbital coefficient plots of the frontier orbitals on the p_z -like orbitals of two hydrogen atoms show this difference at the atomic orbital level. But we cannot find any possible origin from the MOs themselves of alkanethiol, because there is no distinct difference between the LDOS contours of 7- and 8-alkanethiol MOs near the HOMO and LUMO, as Figure 16 shows.

So the origin of the difference between electronic state structures should be traced back to the most obvious distinction

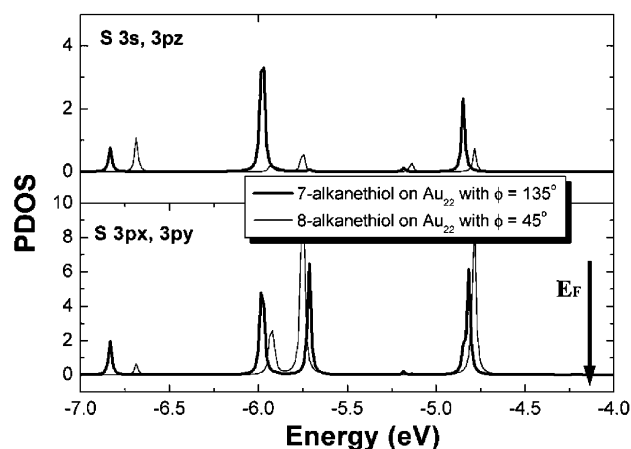


Figure 18. PDOS of 7- and 8-alkanethiol adsorbed at the hcp site of Au(111) and DOS projected onto sulfur 3s and $3p_z$ orbitals with σ symmetry and sulfur 3p_x and 3p_y orbitals with π symmetry. The twist angle ϕ is 45° for 8-alkanethiol, and 135° for 7-alkanethiol. Only the occupied states near E_F are shown.

between two chemisorption structures: the twist angle ϕ of the hydrocarbon chains of alkanethiol. In configurations I, the ϕ values for even and odd carbon atom number are of $\pm 45^\circ$ and $\pm 135^\circ$, respectively. This ensures that the topmost group structures and orientations of two configurations are the same: all are of configurations I. But, it also shows that the adsorption structures and modes of sulfur on the Au(111) surface are different for even- and odd-carbon-atom-number alkanethiol adsorption systems. In fact, Sellers et al.’s ab initio calculation first found the existence of two adsorption modes of the alkanethiol molecule on the Au(111) surface, and they feature sp^3 hybridization and sp hybridization on sulfur, respectively.¹⁷ Although the chemisorption mode for sulfur on Au(111) does not perfectly follow sp^3 and sp hybridization in actual alkanethiol SAMs, the existence of two kinds of distinct chemisorption conformations for sulfur on Au(111) had already been verified by experiments⁷⁴ and MD simulation.^{12,14,16} Our cluster models adopt the result of geometry optimization and MD simulation operated by Li et al.,¹⁶ in which the orientational configurations with $\phi = \pm 45^\circ$ are approximately of sp hybridization, and those with $\phi = \pm 135^\circ$ are approximately of sp^3 hybridization. Figure 18 shows the PDOS of 7- and 8-alkanethiol adsorbed at the hcp site of Au(111), and DOS is projected onto sulfur 3s and $3p_z$ orbitals with σ symmetry and sulfur 3p_x and 3p_y orbitals with π symmetry. In this figure, only the occupied states near E_F are shown, because the difference between the voltage-dependent patterns in our case occurs under negative sample bias voltage. It is found that there exists an obvious difference between two PDOS plots for two chemisorption modes and mainly σ -character of sulfur bonding on Au surface. As the simulated STM images show, the difference between the electronic distributions in the energy and spatial scale for two hybridization configurations is distinct in the region detected by the STM tip. Further, we have calculated the TDOS and PDOS of all orientational configurations with the number of carbon atoms from 6 to 11 and found that the electronic structure near E_F , i.e., the frontier orbitals, is almost determined by only the bonding mode (or hybridization mode) of the sulfur atom. As long as the sulfur atom is fixed on any specific site of the Au(111) surface, the properties of the frontier orbitals are mainly predominated by the ϕ value, and the variety of the number of carbon atoms scarcely influences it. According to our results, it is evident that the chemisorption mode of the alkanethiol

molecule on the Au(111) surface influences the distribution in energy and spatial scale of electronic states.

The influence of the chemisorption mode of the sulfur atom on the distribution of LDOS in energy and spatial scales around another terminal part of the hydrocarbon chain should be limited by the spatial factor; i.e., it maybe has a chain length effect. Our simulated results for long-chain *n*-alkanethiol molecules with $n > 11$ showed the nonsensitivity of STM images on the bias voltage (or energy), which may be interpreted as follows: for a long-chain alkanethiol molecule adsorbed on Au(111), the increment of spatial distance between the Au-bound sulfur atom and the terminal groups results in the chemisorption mode (or hybridization mode) of sulfur hardly affecting the electronic distribution on the scale of space and energy near the terminal groups of the hydrocarbon chain. On the other hand, the disappearance of the odd–even effect for short-chain alkanethiol molecules may be understood as follows: the alkyl chain of the alkanethiol molecule is so short that the interaction between the Au substrate states and alkyl chain also obviously influence the LDOS distribution near the terminal groups of the alkyl chain. Actually, the orientational configurations of alkanethiol SAMs with short chain length are also very complicated due to the dominant sulfur–Au interaction,²² which results in the patterns in STM images also being difficult to theoretically interpret.

The evaluation of other influences of structure parameters of the alkanethiol adsorption system on the pattern in the simulated STM image also illuminates the dominant effect of the chemisorption mode of sulfur on the voltage-dependent pattern in the STM image. The voltage dependences of the patterns in STM images with fcc adsorption sites are different from that with an hcp adsorption site, which is also understandable: on the second Au(111) layer there exists a Au atom just below the sulfur atom for the hcp adsorption site, but no such Au atom exists for fcc adsorption site. This next-nearest neighbor Au atom of the sulfur atom has nonnegligible influence on the chemisorption mode of the sulfur atom. So the movement of the adsorption site of sulfur on Au(111) results in partial change of its chemisorption mode, which causes the difference between the voltage-dependent patterns in the STM image. Similarly, the differences between STM images with a bridge adsorption site and those for hcp site adsorption result from the transformation from the three nearest neighbor Au atoms configuration to the two nearest neighbor Au atoms configuration. The variety of the tilt direction of the alkanethiol molecule does not affect the chemisorption mode of the sulfur atom, so the result that the patterns in the STM images are independent of the tilt direction is not surprising. At last, the $\pm 10^\circ$ variation of the twist angle of the hydrocarbon chains about their molecular axes does not obviously influence the patterns in simulated STM images, which not only ensures that our conclusion is not affected by the error of the twist angle but also re-claims the obvious distinction of two chemisorption modes.

It has already been accepted that a sulfur atom enhances the electronic coupling (or the intermixing degree) between the hydrocarbon chain of an alkanethiol molecule and a Au surface, which helps to produce an appreciable tunneling current.⁶⁸ From the electronic structure analysis for the adsorption system, we also can find that the sulfur atom enhances the intermixing between alkyl part and Au substrate states. More importantly, our above analysis in this subsection shows the sulfur atom has another important effect on STM imaging for alkanethiol SAMs: the different chemisorption modes of sulfur on Au(111) determine different electronic couplings between the

alkanethiol molecule and the Au surface and obviously influence the voltage dependence of the pattern in the STM image, or the electronic distribution in energy and spatial scale around some groups of the terminal part of the hydrocarbon chain. Joachim et al. had also emphasized the important effect of the electronic coupling between the molecule and metal electrode on the conductance and transparency of long molecular wires.⁶⁸

But what mechanism can make the chemisorption mode of sulfur influence the electronic distribution in energy and spatial scale around some groups in the terminal part of the hydrocarbon chain? And how does it transfer the chemisorption information of sulfur to another terminal part through the “blunt” hydrocarbon chain? These questions are interesting and remain open. A possible explanation is the classical induction effect: the chemisorption mode of sulfur determines the ability of attracting electrons for sulfur, and by the induction effect, this kind of ability can influence the polarities of the hydrocarbon chain near sulfur, i.e., the electronic distribution around different CH₂ (or CH₃) groups, so it may be expected that the electronic distributions around some groups are different for different chemisorption modes of sulfur, especially in some MOs (in our case, the difference mainly occurs in the occupied states). The difference between σ -characters of sulfur bonding on the Au surface for two configurations also suggests this point. Generally, the induction effect disappears beyond five atoms in the atom chain. In our case, the odd–even effect of the pattern in occupied STM images disappears for long chain length alkanethiol molecules, which is also consistent with the induction effect. The hyperconjugation effect can also possibly work in this case. Further studies are underway in solving this mechanism question.

E. Characteristics of STM Image for Alkanethiol SAMs.

On the whole, our simulated STM images qualitatively reproduce a majority of characteristics found in STM experiments, especially those employing high tunneling-junction impedance.^{28,29,32,33} For example, our simulated results show that when the carbon atoms number n is increased to 12 and more, the difference between the patterns in simulated STM images under various bias voltage conditions for various orientational configurations gradually becomes inconspicuous and even disappears, which is consistent with almost all experimental reports on the special patterns in STM images of alkanethiol SAMs occurring for short chain *n*-alkanethiol ($n \leq 12$). The analysis of the influence of the tip height on STM image suggests that in STM experiments the information of the first and other CH₂ groups are difficult to detect when the STM tip approaches alkanethiol SAMs. This is consistent with the high tunneling-junction impedance STM experimental results, in which, by decreasing the tunneling current to increase the distance between the STM tip and alkanethiol SAMs, more complex and abundant information was found, especially that the terminal CH₃ group and the first CH₂ group next to it are easy to resolve simultaneously. More importantly, two STM experimental results about the bias voltage dependence of the pattern in the STM image^{30,47} are also consistent with the simulation results in this paper, and they all found that under higher positive sample bias voltage, the pattern of alkanethiol SAMs is no longer a simple round spot.

Our studies not only have validated STM experimental results but also can help to further explore the complicated structure of alkanethiol SAMs on Au(111). By using the bias voltage dependence of the pattern in the STM image, we can distinguish between various orientational configurations of the alkanethiol molecule and will possibly identify the packing configurations of alkanethiol SAMs in STM experiments with higher precision,

even other more general organic molecule materials. Our recent work has begun to realize this possibility.⁴⁷ Another possible use is to determine the adsorption site of sulfur in alkanethiol on a Au surface, which has been always argued as mentioned above. Our simulated results show that the adsorption site of sulfur also affects the bias voltage dependence of the pattern in the STM image. Although this influence may be not very distinct in some cases, it is possible that by operating more elaborate STM experiments, the adsorption site of sulfur in alkanethiol SAMs can be determined by checking the bias voltage dependence of the pattern in the experimental STM images and comparing it with the simulated results.

As a summary we think that the topographic effects dominate the STM images of *n*-alkanethiol SAMs on Au(111) with close-packed hexagonal structure, including: (1) the pattern in the STM image represents the information of the terminal part of the hydrocarbon chain, not that of Au-bound sulfur, and (2) the information of the terminal CH₃ group and the first CH₂ group can be resolved simultaneously in the STM image only for configuration I in which the first CH₂ group is not cloaked by the terminal CH₃ group. The topographic effect is related with the spatial localization of MOs at some groups of the alkyl molecule. But the patterns in images under some tunneling conditions are modulated by the electronic effect: there exist diversities between spatial extensions of different MOs, which results in the first and other CH₂ groups only being detected under appropriate tunneling voltage; also, the adsorption mode of the sulfur atom influences the spatial extensions of these MOs, especially occupied orbitals, which results in the odd-even effect of the bias voltage dependent pattern in STM images for configurations I under negative sample bias voltage.

V. Conclusion

The LDA calculations are performed to simulate the STM image of an alkanethiol molecule in the close-packing upright SAMs on a Au(111) surface. The patterns in the simulated STM images reflect the information of the terminal part of the hydrocarbon in the alkanethiol molecule and possess the voltage dependence and chain-length dependence, especially the odd-even effect when the carbon atom number *n* is from 6 to 11. Further analysis shows that the chemisorption of an alkanethiol molecule on a Au surface results in the intermixing of alkanethiol MOs and Au substrate states with different rates, and new states appearing in the original big energy gap of the alkanethiol contribute to STM imaging near *E_F*. Because the terminal part of the hydrocarbon chain is closer to the STM tip than the Au-bound sulfur, so the simulated STM images are dominated by the information of the alkyl part, though they only contribute a little to those new states. The intermixing of alkanethiol MOs with Au substrate states with different mixing rates induces the energy dependence of the spatial extension of those new states belonging to the adsorption system and brings on the voltage dependence of the simulated STM images. The sulfur atom enhances the intermixing degree between the alkyl states of the alkanethiol molecule and the Au substrate states, and the chemisorption mode of sulfur on the Au surface obviously influences the electronic distribution in energy and spatial scale around some groups of the terminal part of the hydrocarbon chain, which is the origin of the chain-length dependence and odd-even effect in our case. The possible mechanism of transferring this kind of influence through the hydrocarbon chain is attributed to the induction effect. Mainly, our simulated results are consistent with a majority of STM experimental results, especially high tunneling resistance STM experiments.

Acknowledgment. We thank the NSF of China (59972036, 10074059, 19904012, 20025309, 10074058), NKBRSF (G1999075305, G2001CB3095), and the Hong Kong "Qiu Shi" foundation.

References and Notes

- (1) Ulman, A. *An Introduction to Thin Organic Films: From Langmuir-Blodgett to Self-Assembly*; Academic Press: Boston, MA, 1991.
- (2) Laibinis, P. E.; Bain, C. D.; Nuzzo, R. G.; Whitesides, G. M. *J. Phys. Chem.* **1995**, *99*, 7663.
- (3) Haussling, L.; Knoll, W.; Ringsdorf, H.; Schmitt, F.-J.; Yang, J. *Makromol. Chem. Macromol. Symp.* **1991**, *46*, 145.
- (4) Lee, J. H.; Kopecek, J.; Andrade, J. D. *J. Biomed. Mater. Res.* **1989**, *23*, 251. Haussling, L.; Ringsdorf, H.; Schmitt, F.-J.; Knoll, W. *Langmuir* **1991**, *7*, 1837. Collinson, M.; Bowden, E. F.; Tarlov, M. *J. Langmuir* **1992**, *8*, 1247.
- (5) Prasad, P. N.; Williams, D. *Introduction to Nonlinear Optical Effects in Molecules and Polymers*; Wiley-Interscience: New York, 1991.
- (6) Singhvi, R.; Kumar, A.; Lopez, Z. P.; Stephanopoulos, G. N.; Wang, D. I.; Whitesides, G. M.; Ingber, D. E. *Science* **1994**, *264*, 696. Wirth, M. J.; Fairbank, R. W.; Fatunmbi, H. O. *Science* **1997**, *275*, 44.
- (7) Ulman, A. *Thin Films: Self-Assembled Monolayers of Thiols*; Academic Press: San Diego, CA, 1998.
- (8) Ulman, A. *Chem. Rev.* **1996**, *96*, 1533.
- (9) Dubois, L. H.; Nuzzo, R. G. *Annu. Rev. Phys. Chem.* **1992**, *43*, 437.
- (10) Schreiber, F. *Prog. Surf. Sci.* **2000**, *65*, 151.
- (11) Hautman, J.; Klein, M. L. *J. Chem. Phys.* **1989**, *91*, 4994. Hautman, J.; Klein, M. L. *J. Chem. Phys.* **1990**, *93*, 7483.
- (12) Mar, W.; Klein, M. L. *Langmuir* **1994**, *10*, 188.
- (13) Sprik, M.; Delamarche, E.; Michel, B.; Röthlisberger, U.; Klein, M. L.; Wolf, H.; Ringsdorf, H. *Langmuir* **1994**, *10*, 4116.
- (14) Bhatia, R.; Garrison, B. J. *Langmuir* **1997**, *13*, 765. Bhatia, R.; Garrison, B. J. *Langmuir* **1997**, *13*, 4038. Pertsin, A. J.; Grunze, M. *J. Chem. Phys.* **1997**, *106*, 7343.
- (15) Mahaffy, R.; Bhatia, R.; Garrison, B. J. *J. Phys. Chem. B* **1997**, *101*, 771.
- (16) Li, T.-W.; Chao, I.; Tao, Y.-T. *J. Phys. Chem. B* **1998**, *102*, 2935.
- (17) Sellers, H.; Ulman, A.; Shnidman, Y.; Eilers, J. E. *J. Am. Chem. Soc.* **1993**, *115*, 9389.
- (18) Beardmore, K. M.; Kress, J. D.; Jensen, N. G.; Bishop, A. R. *Chem. Phys. Lett.* **1998**, *286*, 40.
- (19) Häkkinen, H.; Barnett, R. N.; Landman, U. *Phys. Rev. Lett.* **1999**, *82*, 3264.
- (20) Grönbeck, H.; Curioni, A.; Andreoni, W. *J. Am. Chem. Soc.* **2000**, *122*, 3839.
- (21) Yourdshahyan, Y.; Zhang, H. K.; Rappe, A. M. *Phys. Rev. B* **2001**, *63*, R081405.
- (22) Akinaga, Y.; Nakajima, T.; Hirao, K. *J. Chem. Phys.* **2001**, *114*, 8555.
- (23) Vargas, M. C.; Giannozzi, P.; Selloni, A.; Scoles, G. *J. Phys. Chem. B* **2001**, *105*, 9509.
- (24) Hayashi, T.; Morikawa, Y.; Nozoye, H. *J. Chem. Phys.* **2001**, *114*, 7615.
- (25) Morikawa, Y.; Hayashi, T.; Liew, C. C.; Nozoye, H. *Surf. Sci.* **2002**, *507-510*, 46.
- (26) Lemay, S. G.; Janssen, J. W.; Hout, M. van den; Mooij, M.; Bronikowski, M. J.; Willis, P. A.; Smalley, R. E.; Kouwenhoven, L. P.; Dekker, C. *Nature* **2001**, *412*, 617.
- (27) Widrig, C. A.; Alves, C. A.; Porter, M. D. *J. Am. Chem. Soc.* **1991**, *113*, 2805.
- (28) Anselmetti, D.; Baratoff, A.; Guntherodt, H. J.; Delamarche, E.; Michel, B.; Gerber, C.; Kang, H.; Wolf, H.; Ringsdorf, H. *Europhys. Lett.* **1994**, *27*, 365. Delamarche, E.; Michel, B.; Gerber, C. *Langmuir* **1994**, *10*, 2869. Delamarche, E.; Michel, B.; Biebuyck, H. A.; Gerber, C. *Adv. Mater.* **1996**, *8*, 719.
- (29) Poirier, G. E.; Tarlov, M. *J. Langmuir* **1994**, *10*, 2853. Poirier, G. E.; Tarlov, M. J.; Rushmeir, H. E. *Langmuir* **1994**, *10*, 3383.
- (30) Bucher, J. P.; Santesson, L.; Kern, K. *Appl. Phys. A* **1994**, *59*, 135.
- (31) Camillone, N., III; Eisenberger, P.; Leung, T. Y. B.; Schwartz, P.; Scoles, G.; Poirier, G. E.; Tarlov, M. *J. Chem. Phys.* **1994**, *101*, 11031.
- (32) Schönenberger, C.; Jorritsma, J.; Sondag-Huethorst, J. A. M.; Fokink, L. G. J. *J. Phys. Chem.* **1995**, *99*, 3259.
- (33) Poirier, G. E.; Pylant, E. D. *Science* **1996**, *272*, 1145.
- (34) Touzov, I.; Gorman, C. B. *J. Phys. Chem. B* **1997**, *101*, 5263.
- (35) Kobayashi, K.; Yamada, H.; Horiuchi, T.; Matsushige, K. *Jpn. J. Appl. Phys.* **1998**, *37*, 6183.
- (36) Arce, F. T.; Vela, M. E.; Salvezza, R. C.; Arvia, A. J. *J. Chem. Phys.* **1998**, *109*, 5703. Arce, F. T.; Vela, M. E.; Salvezza, R. C.; Arvia, A. J. *Langmuir* **1998**, *14*, 7203.

- (37) Voets, J.; Gerritsen, J. W.; Grimbergen, R. F. P.; Kempen, H. van. *Surf. Sci.* **1998**, 399, 316.
- (38) Kondoh, H.; Nozoye, H. *J. Phys. Chem. B* **1999**, 103, 2585.
- (39) Kawasaki, M.; Sato, T.; Tanaka, T.; Takao, K. *Langmuir* **2000**, 16, 1719.
- (40) Vericat, C.; Vela, M. E.; Andreasen, G.; Salvatorezza, R. C.; Vázquez, L.; Martín-Gago, J. A. *Langmuir* **2001**, 17, 4919.
- (41) Dürrig, U.; Züger, O.; Michel, B.; Häussling, L.; Ringsdorf, H. *Phys. Rev. B* **1993**, 48, 1711.
- (42) Salmeron, M.; Neubauer, G.; Folch, A.; Tomitori, M.; Ogletree, D. F.; Sautet, P. *Langmuir* **1993**, 9, 3600.
- (43) Bumm, L. A.; Arnold, J. J.; Dunbar, T. D.; Allara, D. L.; Weiss, P. S. *J. Phys. Chem. B* **1999**, 103, 8122.
- (44) Son, K.-A.; Kim, H. I.; Houston, J. E. *Phys. Rev. Lett.* **2001**, 86, 5357.
- (45) Chiang, S. *Chem. Rev.* **1997**, 97, 1083.
- (46) Sautet, P. *Chem. Rev.* **1997**, 97, 1097.
- (47) Zeng, C. G.; Li, B.; Wang, B.; Wang, H. Q.; Wang, K. D.; Yang, J. L.; Hou, J. G. *J. Chem. Phys.* **2002**, 117, 851.
- (48) Hou, J. G.; Yang, J. L.; Wang, H. Q.; Li, Q. X.; Zeng, C. G.; Lin, H.; Wang, B.; Chen, D. M.; Zhu, Q. S. *Phys. Rev. Lett.* **1999**, 83, 3001.
- (49) Tersoff, J.; Hamann, D. R. *Phys. Rev. Lett.* **1983**, 50, 1998. Tersoff, J.; Hamann, D. R. *Phys. Rev. B* **1985**, 31, 805.
- (50) Chidsey, C. E. D.; Liu, G.-Y.; Rowntree, P.; Scoles, G. *J. Chem. Phys.* **1989**, 91, 4421. Chidsey, C. E. D.; Loiacono, D. N. *Langmuir* **1990**, 6, 682. Chidsey, C. E. D.; Loiacono, D. N. *Langmuir* **1990**, 6, 709. Chidsey, C. E. D.; Liu, G.; Rowntree, P.; Scoles, G. *J. Chem. Phys.* **1998**, 91, 4421.
- (51) Nuzzo, R. G.; Dubois, L. H.; Allara, D. L. *J. Am. Chem. Soc.* **1990**, 112, 558. Nuzzo, R. G.; Korenic, E. M.; Dubois, L. H. *J. Chem. Phys.* **1990**, 93, 767.
- (52) Camillone, N.; Chidsey, C. E. D.; Liu, G.-Y.; Scoles, G. *J. Chem. Phys.* **1993**, 98, 4234. Camillone, N.; Chidsey, C. E. D.; Liu, G.; Scoles, G. *J. Chem. Phys.* **1993**, 98, 3503.
- (53) Fenter, P.; Eisenberger, P.; Liang, K. S. *Phys. Rev. Lett.* **1993**, 70, 2447.
- (54) Dubois, L. H.; Zegarski, B. R.; Nuzzo, R. G. *J. Chem. Phys.* **1993**, 98, 678.
- (55) Biebuyck, H. A.; Bain, C. D.; Whitesides, G. M. *Langmuir* **1994**, 10, 1825.
- (56) Carron, K. T.; Hurley, G. J. *J. Phys. Chem.* **1991**, 95, 9979.
- (57) Kato, H. S.; Noh, J.; Hara, M.; Kawai, M. *J. Phys. Chem. B* **2002**, 106, 9655.
- (58) Fenter, P.; Eberhardt, A.; Liang, K. S.; Eisenberger, P. *J. Chem. Phys.* **1997**, 106, 1600.
- (59) Fenter, P.; Eberhardt, A.; Eisenberger, P. *Science* **1994**, 266, 1216.
- (60) Yeganeh, M. S.; Dougal, S. M.; Polizzotti, R. S.; Rabinowitz, P. *Phys. Rev. Lett.* **1995**, 74, 1811.
- (61) Gerdy, J. J.; Goodard, W. A. *J. Am. Chem. Soc.* **1996**, 118, 3233.
- (62) Kluth, G. J.; Carraro, C.; Maboudian, R. *Phys. Rev. B* **1999**, 59, R10449.
- (63) Kohn, W.; Sham, L. J. *Phys. Rev.* **1965**, 140, A1133. Kohn W.; Sham, L. J. *Phys. Rev.* **1966**, 145, A561.
- (64) Dmol Version 960, Density Functional Theory electronic structure program, Copyright 1996 by Molecular Simulations, Inc.
- (65) Vosko, S. J.; Wilk, L.; Nusair, M. *Can. J. Phys.* **1980**, 58, 1200.
- (66) Ceperley, D. M.; Alder, B. J. *Phys. Rev. Lett.* **1980**, 45, 566.
- (67) Clarke, A. R. H.; Pethica, J. B.; Nieminen, J. A.; Besenbacher, F.; Lægsgaard, E.; Stensgaard, I. *Phys. Rev. Lett.* **1996**, 76, 1276. Olesen L.; Brandbyge, M.; Sørensen, M. R.; Jacobsen, K. W.; Lægsgaard, E.; Stensgaard, I.; Besenbacher, F. *Phys. Rev. Lett.* **1996**, 76, 1485.
- (68) Joachim, C.; Vinuesa, J. F. *Europhys. Lett.* **1996**, 33, 635. Magoga, M.; Joachim, C. *Phys. Rev. Lett.* **1997**, 56, 4722.
- (69) Kondoh, H.; Kondama, C.; Sumida, H.; Nozoye, H. *J. Chem. Phys.* **1999**, 111, 1175.
- (70) Staub, R.; Toerker, M.; Fritz, T.; Schmitz-Hübsch, T.; Sellam, F.; Leo, K. *Langmuir* **1998**, 14, 6693.
- (71) Camillone, N.; Leung, T. Y. B.; Schwartz, P.; Eisenberger, P.; Scoles, G. *Langmuir* **1996**, 12, 2737.
- (72) Faglioni, F.; Claypool, C. L.; Lewis, N. S.; Goddard, W. A., III *J. Phys. Chem. B* **1997**, 101, 5996.
- (73) Eigler, D. M.; Weiss, P. S.; Schweizer, E. K. *Phys. Rev. Lett.* **1991**, 66, 1189.
- (74) Heister, K.; Zharnikov, M.; Grunze, M.; Johansson L. S. O. *J. Phys. Chem. B* **2001**, 105, 4058.